15.2 CLOUD STRUCTURES, MICROPHYSCIAL PROCESSES AND SYNERGISTIC INTERACTIONS BETWEEN FRONTAL AND OROGRAPHIC FORCING OF PRECIPITATION

Christopher P. Woods, Mark T. Stoelinga, John D. Locatelli, Peter V. Hobbs*
University of Washington, Seattle, WA

1. INTRODUCTION

The orographic field phase of the University of Washington's (UW) IMPROVE Project focused on the acquisition of comprehensive measurements of meteorological state parameters, polarization Doppler radar measurements, and cloud microphysical parameters to improve understanding of orographically-influenced precipitation. The Oregon Cascades, a north-south mountain barrier in west-central Oregon, is the main topographical feature that modifies cloud processes and precipitation in this region of the Pacific Northwest. Results from an earlier study in the Washington Cascades (Hobbs et al. 1975), as well as orographic studies in other locations (e.g., Reynolds and Dennis 1986), revealed the complexity of storm systems modified by terrain in the western United States. Through the use of a new generation of in-situ and remote sensing instruments in IMPROVE, we hope to add to the knowledge gained in these earlier studies and thereby improve the representations of cloud and precipitation processes in mesoscale models (Stoelinga et al. 2003).

In this paper we summarize data collected during the passage of a strong precipitation system over the Oregon Cascades on 13-14 December 2001. We focus on differentiating between the influences of baroclinic and orographic lifting to the overall precipitation production over the mountains by considering data in reference frames relative to an upper-level baroclinic zone and to the underlying topography. Analysis of ground-based raingauge and microwave radiometrically derived cloud liquid water depth (LWD) measurements enabled quantitative estimation of the synergistic interaction that occurred between precipitation forced frontally and orographically as the system approached and passed over the Oregon Cascade Mountains.

2. DATA

The north-south oriented Oregon Cascade Mountains are located about 150 km east of the Pacific Coast (Fig. 1). The NCAR S-band dual-polarized (S-Pol) radar, which was located about 80 km west of the Cascade ridge, provided coverage across the study area including both the Willamette Valley to the west and the Cascades to the east. This radar was used for long-range weather surveillance, directing aircraft into precipitation features, and for the measurement of reflectivity, polarimetric, and air motions in precipitation features that developed in the study area.

Two aircraft were used in the field study: the NOAA P-3, which provided airborne doppler radar coverage, and the UW's Convair-580 for collecting in-situ cloud microphysical data. The Convair-580 performed a flight pattern consisting of vertically stacked horizontal legs that closely paralleled the cross-barrier flow in order to produce vertical cross-sections of microphysical information.

Special rawinsondes launched from Salem, Oregon, by the National Weather Service, and those from a UW mobile station sonde launch site near Creswell, Oregon, were utilized to deduce the vertical structure of the storm system. Other instrumentation and observational assets included: a snow crystal observational site along the Cascade crest, a series of raingauges extending west-east across the study area, a vertically pointing S-Band radar, and a scanning microwave radiometer for measuring column integrated cloud LWD on the windward side of the barrier.

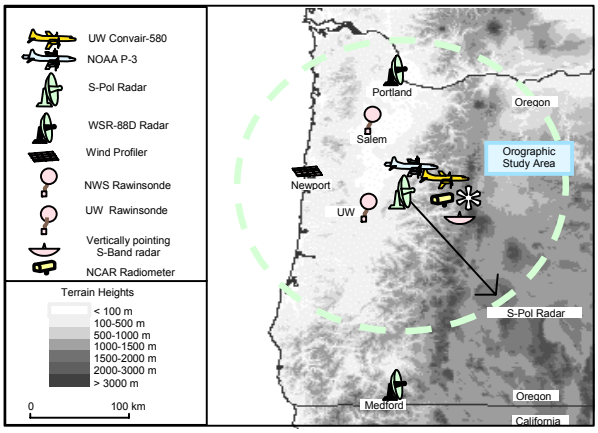

Figure 1. Study area and instrumentation

3. SYNOPTIC DESCRIPTION

A frontal system approached the Pacific Northwest on 13-14 December 2001, as indicated by the strengthening of the 500 hPa trough situated near Vancouver Island at 0000 UTC 14 December. Satellite imagery shows a broad cloud shield associated with this system, extending from the Pacific Coast to western Montana, which was associated with a 981-hPa surface low-pressure center (Fig. 2). There was an upper-level, strong baroclinically-forced rainband ahead of the surface frontal rainband as it progressed across the study area. Cross-barrier flow (25-30 m s^{-1} at 850 hPa) was present throughout the region, which provided strong orographic forcing.

To better understand the overall structure of this storm, a time-height cross-section of rawinsonde data is shown in Fig. 3a. Radar data indicated that a broad rainband, oriented in a southwest-northeast direction, moving at 13.3 m s^{-1} extended ahead of the surface front. This rainband played a significant role in producing precipitation over the Cascades. Since the rainband was associated with an upper-level baroclinic zone,

*Corresponding author address: Peter V. Hobbs, Univ. of Washington, Atmos. Sciences Dept., Seattle, WA 98195-1640; email: phobbs@atmos.washington.edu

the cross-section in Fig. 3a has been assembled so that it is quasi-perpendicular to this rainband. This aids in separating influences resulting from the upper-level baroclinic forcing, and those of orographic forcing on precipitation over the mountains.

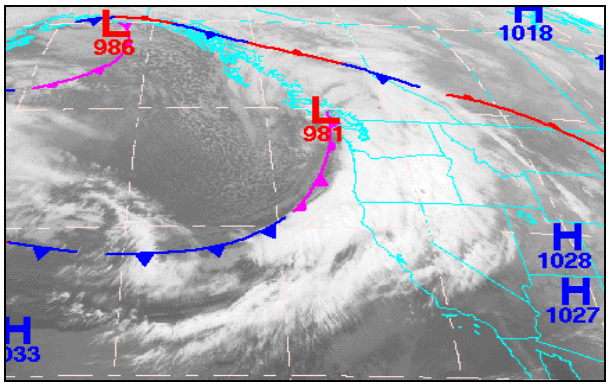

Figure 2. Satellite imagery and NCEP frontal analysis for 0000 UTC 14 December 2001

The cross-section in Fig. 3a shows the tipped-forward orientation of the lower-tropospheric front as it extends upward to an upper-level baroclinic feature above 600 hPa. Equivalent potential temperature contours ahead of the frontal feature indicate the presence of a strong moisture field below and preceding the upper-level baroclinic region, with drier cooler air advecting into the area following its passage. Reflectivity measurements from the vertically pointing S-band radar (see Fig. 1 for location) are shown in Fig. 3b and show the progression of five different precipitation regimes (labeled on the plot) that passed over the Cascades during the storm. We now describe the cloud structures associated with the different time periods, and relate the influences of baroclinic and orographic effects on the microphysical processes important for precipitation production across the study area.

4. CLOUD AND PRECIPITATION STRUCTURES

Evolving cloud structures occurred throughout the passage of the precipitation system. Flight transcripts from the Convair-580 during this time period, along with radar coverage, showed that three main cloud components were present in this case study: a broad altostratus cloud shield associated with the upper-level, baroclinically-forced precipitation band; a low-level stratocumulus orographic cloud, produced by the strong flow across the mountains; and non-orographic convective clouds that formed in the intra-frontal region between the passage of the upper-level band and the surface front, and in the post-frontal conditions.

The altostratus cloud deck that accompanied the upper-level baroclinic forcing was deep and diffuse in nature. The altostratus cloud had tops around 8-9 km and extended down to about 4 km. While this cloud lacked high liquid water contents, the existence of occasional embedded droplet clouds indicated a relatively high level of saturation throughout the altostratus cloud along the Convair-580 flight legs between 6 km and 4 km.

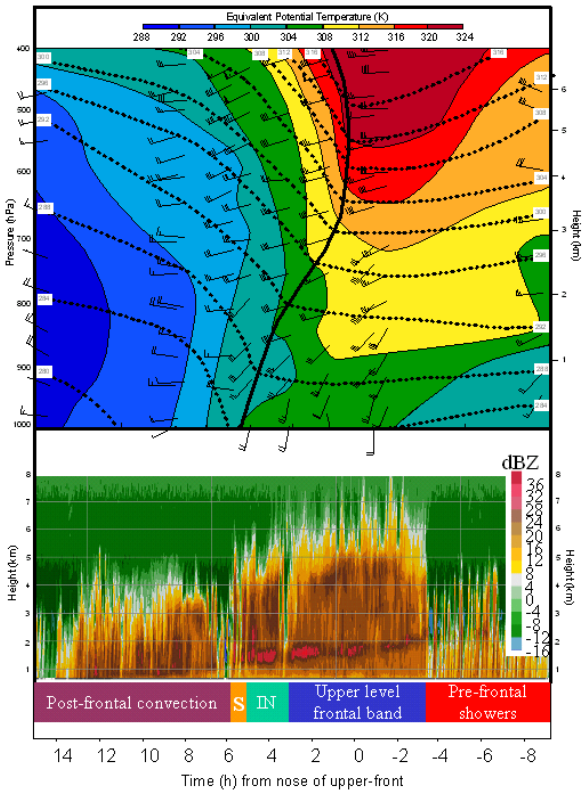

Figure 3. (a) Time-height cross-section based on sondes launched from Salem and Creswell, Oregon (see Fig. 1 for locations). Contours show potential temperature (dashed lines), equivalent potential temperature (shaded) and wind speed (full barb indicates 10 m s^{-1}). Sonde launch times correspond to locations of wind readings shown. (b) Reflectivity (dBZ) from the vertically-pointing S-band radar located at McKenzie Bridge on the windward side of the Oregon Cascade Mountains (see Fig. 1 for location). Precipitation regimes discussed in text are labeled ('Pre-frontal showers', 'Upper-level frontal band', 'IN' (Intra-frontal convection), 'S' (Surface frontal band), and 'Post-frontal convection.'

At lower levels, the primary cloud structure was orographically influenced, as strong upslope flow resulted in the formation of stratocumulus clouds above the barrier. The stratocumulus extended up to the base of the altostratus cloud shield as it passed through the study area. The top of the orographic stratocumulus cloud was capped near the 4 km level by the advection of cold dry air behind the migratory upper-level cloud shield. Scientists aboard the Convair-580 reported small-scale cloud turrets within the orographic cloud; these turrets produced pockets of increased cloud liquid water. The presence of this liquid-water rich orographic cloud played a significant role in the production of precipitation during the storm. Convective clouds, with tops near 4 km, dominated the time period after the passage of the upper-level cloud shield and prior to the passage of the surface frontal rainband. Shallower convection was present in the post-frontal regime, as tops subsided to 2-3 km.

Because strong, moist cross-barrier flow persisted as the upper front passed over the barrier, this allowed for heavy natural seeding of ice particles from above of the orographic

liquid water cloud below. The advantage (for precipitation production) of this configuration is illustrated in the schematic shown in Fig. 4. In this figure, four hypothetical cases are illustrated for a cold front passing over the Cascade Mountains, comprising the four possible combinations of pre-frontal low-level easterly vs. westerly flow and the lower-tropospheric portion of the front being tipped backward or forward. In each case, a middle-to-upper level tropospheric altostratus cloud deck, produced by frontal lifting, generates ice crystals, which fall into the lower troposphere.

In panel (a) of Fig. 4, low-level easterly flow leads to a lack of orographic liquid water cloud ahead of the front. Therefore, pre-frontal precipitation is not enhanced by riming or additional vapor diffusion due to orographic lift in the lower levels. Immediately behind the front, the low-level flow turns westerly, resulting in some low-topped orographic cloud and the possibility of riming and additional diffusional growth of ice particles falling from the upper rear portion of the precipitation band produced by the front. After frontal passage (not shown in Fig. 4), precipitation production is purely orographic in the post-frontal westerlies. Panel (a) of Fig. 4 represents the typical situation discussed by Hobbs (1975) for the Washington Cascades.

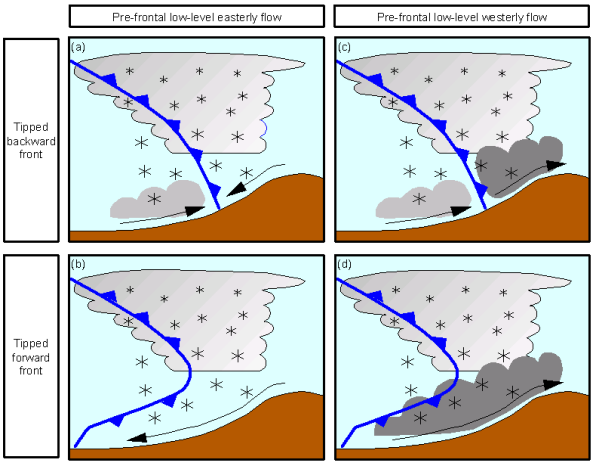

Figure 4. Schematic representation of possible frontal structures and cloud liquid water production above a mountain barrier in response to various low-level flow patterns. Darkly shaded regions indicate clouds with the highest cloud liquid water. (a) For a tipped backward front and pre-frontal easterly flow. (b) As in (a), but for a tipped forward front. (c) For a tipped backward front and pre-frontal westerly flow. (d) As in (c), but for a tipped forward front.

In panel (b) of Fig. 4, the situation is similar to panel (a), except that the front is tipped forward. In this case, there is no low-level upslope flow underneath the upper-level generated precipitation because the pre-frontal low-level easterly flow extends west all the way to the surface front, precluding the development of significant liquid water cloud at low levels and orographic precipitation enhancement. This scenario has not been documented in the literature, although tipped-forward fronts with pre-frontal easterly (or southeasterly) flow are common in the Pacific Northwest (e.g., the IMPROVE-1 case discussed by Locatelli et al. 2005 and Evans et al. 2005).

Panel (c) is similar to panel (a) in Fig. 4, except the pre-frontal flow is now a warm, moist southwesterly flow, leading to a deep orographic cloud rich in liquid water. However, only some of the ice precipitation from the frontal band aloft falls into this cloud. Much of it falls behind the front, into the shallower post-frontal orographic cloud. This frontal structure and lower-level flow pattern are similar to the 8-9 December 2001 IMPROVE-2 event described by Bond et al. (2005).

Finally, the combination that leads to the greatest potential for precipitation production is shown in Fig. 4 panel (d), in which strong, moist southwesterly low-level flow leads to a deep orographic cloud rich in liquid water, and this cloud exists beneath the entire frontally-driven precipitation band due to the tipped-forward configuration of the front. This results in maximum overlap of ice precipitation from the frontal band aloft and the deep orographic cloud below; a situation that is conducive for ice particles produced aloft to naturally seed the orographic cloud below. The scenarios shown in panel (b) and (d) of Fig. 4 are similar in many ways to a common scenario in the Sierra Nevada of California. Heggli and Reynolds (1985), Reynolds and Kuciauskas (1988), and Heggli and Rauber (1988) found that several storm systems studied during the Sierra Cooperative Pilot Project (Reynolds and Dennis 1986) fit the "split-front" conceptual model of Browning and Monk (1982), in which an upper cold front leads the passage of the front at the surface. Although they did not specifically show the low-level wind field across the barrier in the pre-frontal environment, other aspects of the cases they described imply upslope flow at all levels in the pre-frontal environment, which is consistent with Fig. 4d.

5. SYNERGISTIC INTERACTION

One way to describe the interaction between frontal and orographic precipitation processes is as a synergistic interaction. In other words, the combination of these two processes is likely to yield a larger amount of precipitation than would either process acting alone. The synergistic effect arises primarily from an additional "seeder-feeder" (Bergeron 1950) contribution to precipitation, whereby ice particles produced in frontal precipitation bands aloft fall into liquid orographic cloud, removing (through both the vapor diffusion and riming) cloud water that would otherwise not have been removed. Many studies have provided evidence for these synergistic processes. However, it has been difficult to quantify the synergistic effect due to an inability to quantify the contribution of either process (frontal dynamics and orographic lifting) to precipitation growth in isolation from the other. We will now estimate this synergistic effect for the 13-14 December 2001 case described in this paper.

A dual-channel microwave radiometer, deployed by NCAR on the ground just upstream of the Cascade crest at an elevation of 1138 m (see Fig. 1 for location), provided measurements of vertically-integrated CLW (expressed as equivalent liquid water depth, LWD) throughout the passage of the 13-14 December 2001 storm. The radiometer was equipped with an internal heater and an external heater/fan that blew warm air onto the exterior cover to keep it free of liquid wa-

ter, snow, and ice. As frontal features passed over the radiometer site, fluctuations were seen in the LWD (Fig. 5).

In the presence of rain, two sources of uncertainty are introduced in interpreting the radiometrically retrieved LWD as an accurate measurement of cloud LWD. First, the radiometer does not distinguish between cloud and rainwater. Therefore, the rainwater in the column contributes to the column-integrated measurement. Second, the retrieval algorithm is not valid for rain-sized water droplets (see, for example, Czekala et al. 2001). During much of the period of precipitation discussed in this paper, rain occurred at the radiometer site. To address the first issue, we estimated the portion of liquid water in the column due to rain by estimating the depth of the rain layer and the concentration of rainwater within that layer. The rain layer was assumed to extend from ground level at the radiometer location to the melting level, as indicated by the bright band measured by the nearby vertically pointing S-band radar (Fig. 3b). The rain concentration within the rain layer was estimated from the rain rate, measured by a raingauge collocated with the radiometer, using the Marshall-Palmer (1948) distribution. From this estimate (shown in Fig. 5) it can be seen that the rainwater contribution to the LWD was small compared to the total radiometrically retrieved LWD. The other issue is the error in the retrieval algorithm due to rainwater. A recent study by Löhnert and Crewell (2003) suggests that for liquid water path (LWP) values such as those encountered in the present study (~ 1.0 mm), errors in rainy conditions may be as large as 0.3 mm, and are usually overestimates. Thus, when interpreting the black curve in Fig. 5 as cloud LWP, it should be understood that those values may be overestimates of cloud LWP by up to 0.3 mm during the period of rain. However, we will hereafter assume the black curve in Fig. 5 depicts cloud LWD.

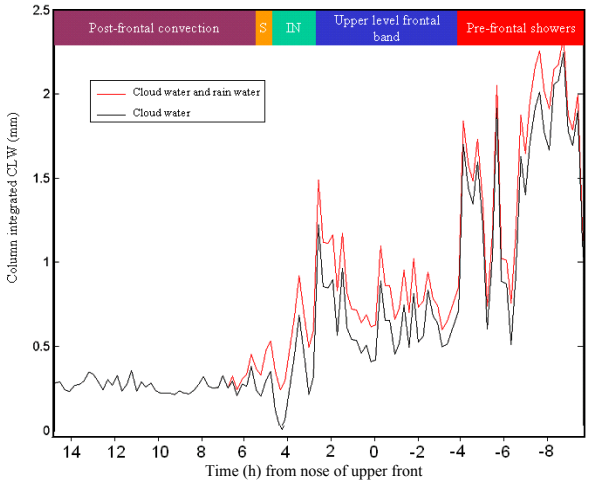

Figure 5. Vertically integrated cloud liquid water (CLW) from the NCAR radiometer (see Fig. 1 for location) expressed as cloud liquid water depth (LWD) and projected onto the time-height coordinates in Fig. 3. Sum of rain and cloud water (dotted line), and cloud water only (solid line). Precipitation regimes (see Fig. 3) are indicated.

Comparison of the LWD near crest level (Fig. 5) during the pre-frontal showers regime and the upper-level baroclinically forced rainband regime indicated a decrease in CLW of ~ 0.8 mm, despite similar upstream moisture content and cross-barrier flow during these two time periods. Therefore, one estimate of the synergistic effect would be a steady removal of this amount of CLW over the upslope zone. If we assume that a difference of 0.8 mm of CLW is produced and fully scavenged between the initial Cascade upslope and the mountain crest, the timescale necessary for CLW production and depletion can be estimated by using the mean lower-level (1-2 km) cross-barrier wind component (~ 27 m s^{-1}) and the distance between the initial upslope and Cascade crest (~ 80 km). The resulting increase in precipitation due to enhanced CLW scavenging between the pre-frontal precipitation regime and the precipitation associated with the upper-band regime is ~ 1.0 mm h^{-1}, which would represent an average value over the entire upslope zone. It also probably represents an upper bound, since not all of the "missing" CLW necessarily went into additional precipitation fallout.

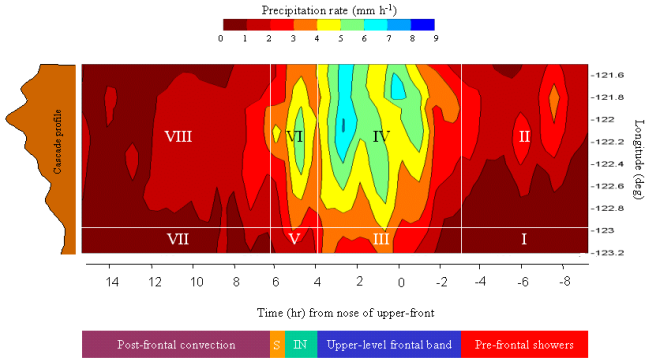

Figure 6. Contour plot of precipitation rate (mm h^{-1}) from ground-based raingauges, in a time-space reference frame with the time axis the same as in Fig. 3. The Oregon Cascade mountain profile is also shown. Precipitation regimes are shown as in Fig. 3 and regions I-VIII discussed in text are labeled.

A second estimate can be obtained by examining ground-based precipitation measurements for the event using the time-space analysis technique described by Hobbs et al. (1975). From Fig. 6 we can estimate average precipitation amounts in the various precipitation regimes relative to the frontal structure, as well as relative to the various orographic zones. Precipitation during the passage of the upper-level band over the upslope zone (region IV in Fig. 6) resulted from both baroclinic and orographic forcing. Since similar upstream moisture and cross-barrier flow existed in the lower-troposphere over the upslope zone during the 'pre-frontal showers' and 'upper-level frontal band' regimes, we use the precipitation in region II (Fig. 6) to represent the contribution due to orographic forcing alone. Precipitation due to baroclinic forcing alone is estimated from the rainfall that occurred during the passage of the upper-frontal rainband over the flat Willamette Valley west of the Cascade Range (region III in Fig. 6). This estimate relies on the assumptions of limited orographic influence over the Willamette Valley, and the approximately steady-state nature of the upper-frontal band as it passed from the Willamette Valley to the Cascade Range. Both of these assumptions appear to be qualitatively valid based on examination of radar data, which showed no evidence of precipitation enhancement over the valley, and a lack of significant transient features within the upper-frontal band.

Thus, the precipitation due to the upper-frontal precipitation band alone, orographic forcing alone, and the combination of the two are estimated from area averages of the precipitation in regions III, II, and IV, respectively. The synergistic contribution would then be the precipitation produced by both processes together (i.e., 4.1 mm h^{-1} from region "IV" in Fig. 6) minus the sum of the precipitation produced by both processes in isolation (i.e., 3.7 mm h^{-1} from the sum of regions "II" and "III" in Fig. 6). This estimate yields a synergistic effect of ~ 0.4 mm h^{-1}. Thus, when considered together, the estimates based on radiometer measurements and raingauge measurements suggest that the synergistic effect is probably in the range of ~ 0.4-1.0 mm h^{-1}, averaged over the orographic precipitation zone. If the synergistic effect is as large as 1 mm h^{-1}, it represents a 60% augmentation of the precipitation produced by orographic processes alone, which is significant from a quantitative precipitation forecasting perspective. Mesoscale model representations of the 13–14 December 2001 IMPROVE-2 event (Colle et al. 2005; Garvert et al. 2005a,b) provide further insights into the cloud and precipitation features described in this paper and in the future will be used to assess the synergism between frontal and orographic precipitation.

6. CONCLUSIONS

A strong cyclonic storm that impinged on the Oregon Cascades on 13-14 December 2001 has provided interesting details related to orographic influences on baroclinically forced precipitation. A comprehensive dataset, comprised of in situ measurements collected from two aircraft and ground-based in situ and remote sensing measurements, has permitted detailed analysis of the storm as it approached and passed over the mountain barrier. The data also provided information on cloud and precipitation processes produced by the interactions of baroclinic and orographic forcing.

The storm was characterized by a tipped-forward, lower-tropospheric frontal zone that extended upward to a backward-tilted upper-level baroclinic zone. As the frontal feature passed over the Oregon Cascades, strong low-level westerly flow that supported enhanced cloud liquid water in the orographic lifting zone occurred simultaneously with enhanced ice crystal production aloft. Ground-based cloud liquid water measurements suggested enhanced scavenging of liquid water by the ice crystals from aloft. Evidence of such scavenging was also provided by ground-based ice crystal observations, which showed primarily heavily rimed ice crystals.

Our investigation suggests that storms which cross the Oregon Cascade Mountains and have similar structures to the case presented here (i.e., a tipped-forward lower-tropospheric front, low-level moist cross-barrier flow, and ice crystal generation at upper-levels preceding the surface front) will likely experience synergistic interactions between frontal and orographic precipitation.

7. ACKNOWLEDGMENTS

Research supported by grant ATM-9632580 from the Mesoscale Dynamic Meteorology Program, Atmospheric Sciences Division, NSF.

8. REFERENCES

Bergeron, T., 1950: Uber der mechanisms ausgiebigen Niederschlage. *Ber. Deut. Wetterd.*, **12**, 225–232.

Bond, N. A., B. F. Smull, M. T. Stoelinga, C. P. Woods, A. Haase, and J. D. Locatelli, 2005: The evolution of a cold front over quasi-2D terrain: Coordinated aircraft observations of the 8-9 December 2001 wide cold frontal rainband during IMPROVE-2. Submitted for publication to the *J. Atmos. Sci.* (IMPROVE Special Issue).

Browning, K. A., and G. A. Monk, 1982: A simple model for the synoptic analysis of cold fronts. *Quart. J. Roy. Meteor. Soc*., **101**, 893–900.

Colle, B. A., M. F. Garvert, J. B. Wolfe, and C. F. Mass, 2005: Microphysical budgets and sensitivity studies for the 13-14 December 2001 IMPROVE-2 event. Submitted for publication to the *J. Atmos. Sci.* (IMPROVE Special Issue).

Czekala, H., S. Crewell, C. Simmer, A. Thiele, A. Hornbostel, and A. Schroth, 2001: Interpretation of polarization features in ground-based microwave observations as caused by horizontally aligned oblate raindrops. *J. Appl. Meteor.*, **40**, 1918–1932.

Evans, A. G., J. D. Locatelli, M. T. Stoelinga, and P. V. Hobbs, 2005: The IMPROVE-1 storm of February 1–2, 2001. Part II: Cloud structures and the formation of precipitation. Accepted for publication to the *J. Atmos. Sci.* (IMPROVE Special Issue).

Garvert, M. F., B. A. Colle, and C. F. Mass, 2005a: Synoptic and mesoscale evolution of the 13-14 December 2001 IMPROVE II storm system and comparison with a mesoscale model simulation. Submitted for publication to the *J. Atmos. Sci.* (IMPROVE Special Issue).

_____, C. P. Woods, B. A. Colle, C. F. Mass, P. V. Hobbs and J. B. Wolfe, 2005b: Comparisons of MM5 model simulations of clouds and precipitation with observations for the 13-14 December 2001 IMPROVE-2 event. Submitted for publication to the *J. Atmos. Sci.* (IMPROVE Special Issue).

Heggli, M. F., and D. W. Reynolds, 1985: Radiometric observations of supercooled liquid water within a split front over the Sierra Nevada. *J. Climate Appl. Meteor.*, **24**, 1258–1261.

_____, and R. Rauber, 1988: The characteristics and evolution of supercooled water in wintertime storms over the Sierra Nevada: A summary of microwave radiometric measurements taken during the Sierra Cooperative Pilot Project. *J. Appl. Meteor.*, **27**, 989–1015.

Hobbs, P.V., R.A. Houze, and T.J. Matejka, 1975: The dynamical and microphysical structure of an occluded frontal system and its modification by orography. *J. Atmos. Sci*., **32**, 1542-1562.

Locatelli, J. D., M. T. Stoelinga, M. F. Garvert, and P. V. Hobbs, 2005: The IMPROVE-1 storm of February 1–2, 2001. Part I: Development of a forward-tilted cold front and a warm occlusion. Submitted for publication to the *J. Atmos. Sci.* (IMPROVE Special Issue).

Löhnert, U., and S. Crewell, 2003: Accuracy of cloud liquid water path from ground-based microwave radiometry. Part I. Dependency on cloud model statistics. *Radio Sci.*, **38**, art. no. 8041.

Marshall, J.S., and W. M. Palmer, 1948: The distribution of raindrops with size. *J. Atmos. Sci.,* **5**, 165-166.

Reynolds, D. W., and A. S. Dennis, 1986: A review of the Sierra Cooperative Pilot Project. *Bull. Amer. Meteor. Soc*., **67**, 513–523.

_____, and A. P. Kuciauskas, 1988: Remote and in situ observations of Sierra Nevada winter mountain clouds: relationships between mesoscale structure, precipitation and liquid water. *J. Appl. Meteor*., **27**, 140–156.

Stoelinga, M. T., P. V. Hobbs, C. F. Mass, J. D. Locatelli, B. A. Colle, R. A. Houze, Jr., A. L. Rangno, N. A. Bond, B. F. Smull, R. M. Rasmussen, G. Thompson, and B. R. Colman, 2003: Improvement of microphysical parameterization through observational verification experiment. *Bull. Amer. Meteor. Soc.*, **84**, 1807-1826.